

Persistence of the Isotopic Signature of Pentavalent Uranium in Magnetite

Zezen Pan, Yvonne Roebbert, Aaron Beck, Barbora Bartova, Tonya Vitova, Stefan Weyer, and Rizlan Bernier-Latmani*



Cite This: <https://doi.org/10.1021/acs.est.1c06865>



Read Online

ACCESS |



Metrics & More

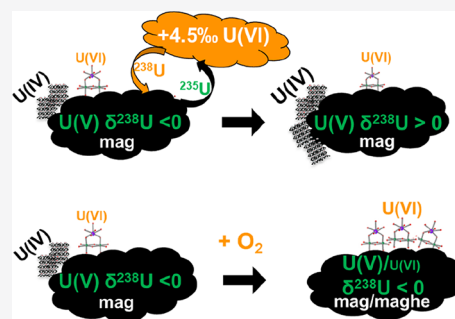


Article Recommendations



Supporting Information

ABSTRACT: Uranium isotopic signatures can be harnessed to monitor the reductive remediation of subsurface contamination or to reconstruct paleo-redox environments. However, the mechanistic underpinnings of the isotope fractionation associated with U reduction remain poorly understood. Here, we present a coprecipitation study, in which hexavalent U (U(VI)) was reduced during the synthesis of magnetite and pentavalent U (U(V)) was the dominant species. The measured $\delta^{238}\text{U}$ values for unreduced U(VI) ($\sim -1.0\text{‰}$), incorporated U ($96 \pm 2\%$ U(V), $\sim -0.1\text{‰}$), and extracted surface U (mostly U(IV), $\sim 0.3\text{‰}$) suggested the preferential accumulation of the heavy isotope in reduced species. Upon exposure of the U-magnetite coprecipitate to air, U(V) was partially reoxidized to U(VI) with no significant change in the $\delta^{238}\text{U}$ value. In contrast, anoxic amendment of a heavy isotope-doped U(VI) solution resulted in an increase in the $\delta^{238}\text{U}$ of the incorporated U species over time, suggesting an exchange between incorporated and surface/aqueous U. Overall, the results support the presence of persistent U(V) with a light isotope signature and suggest that the mineral dynamics of iron oxides may allow overprinting of the isotopic signature of incorporated U species. This work furthers the understanding of the isotope fractionation of U associated with iron oxides in both modern and paleo-environments.



KEYWORDS: pentavalent uranium, isotope fractionation, uranium remediation, redox tracer

INTRODUCTION

Uranium (U) is a contaminant of concern in the subsurface as a result of mining and processing the U ore and improper storage of nuclear waste.^{1,2} Hexavalent U (U(VI)) is largely soluble as it typically exists as uranyl solution complexes with carbonate or organic ligands. In contrast, tetravalent U (U(IV)) is sparingly soluble under anoxic conditions. U(VI) can be reduced to U(IV) through biotic transformation by microorganisms as well as abiotic reduction by Fe(II)- or sulfide-bearing minerals.^{3–5} The stimulation of biological activity in the subsurface has been used as a strategy for the in situ immobilization of U.^{6,7} However, monitoring the U(VI) concentration in the groundwater is not a sufficient indicator of the processes underway as it integrates reduction, dissolution, adsorption, and desorption, with the latter three having limited relevance to remediation efforts.

Thus, U isotope fractionation (based on changes in the uranium isotope ratio $^{238}\text{U}/^{235}\text{U}$) has been used to follow the progression of U bioreduction *in situ*.^{8,9} Based on *ab initio* calculations,¹⁰ the equilibrium isotopic fractionation associated with the reduction of U(VI) to U(IV) favors the accumulation of the heavy isotope (^{238}U) in the U(IV) product. This is opposite to the direction expected for traditional mass-dependent stable isotope fractionation due to the nuclear field shift (NFS).^{10–12} Thus, reduction is often invoked as the

source of U isotope fractionation when a heavy isotope signature is detected in sediments.^{13–18} Additionally, the isotopic signature of U serves as a paleo-redox proxy in a variety of low-temperature paleo-environments^{16,19–22} and modern analogues^{15,17,23,24} to constrain global atmospheric and oceanic redox chemistry variations. The enrichment of ^{238}U has been identified in geological samples (e.g., black shales),²⁵ and the decrease of $^{238}\text{U}/^{235}\text{U}$ in aqueous U(VI) documented in groundwater during bioremediation or from laboratory microbial experiments.^{8,26–29} While monitoring the U isotope ratio rather than U concentration may represent a superior strategy to pinpoint U reduction,⁸ there remain significant uncertainties as to the mechanistic underpinnings of uranium's isotopic fractionation behavior, particularly in the solid phase and in association with iron oxides.

U redox transformation can be coupled to the iron redox cycle. For instance, aqueous-phase U can be captured by iron oxides through adsorption, surface reduction, and incorpo-

Received: October 11, 2021

Revised: January 3, 2022

Accepted: January 5, 2022

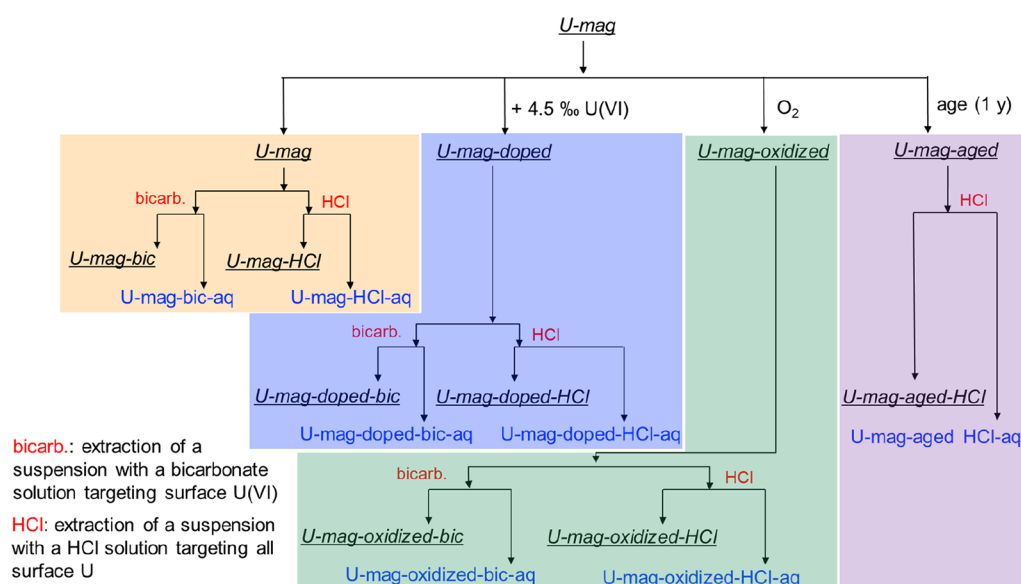


Figure 1. Schematic of the experiment. *U-mag* represents the original coprecipitated suspension; “-aq” represents the extracted aqueous phase after extraction with a bicarbonate (“-bic-aq”) or a HCl (“-HCl-aq”) solution; “-bic” represents the remaining solid phase after bicarbonate extraction and (“-HCl”) after HCl extraction. Here, aqueous samples are represented in blue text and solid samples in underlined black italics text. For example, *U-mag-HCl* represents the solid-phase sample after extraction of the *U-mag* suspension with a HCl solution; meanwhile, *U-mag-HCl-aq* represents the corresponding extracted aqueous phase.

ration during coprecipitation with magnetite or during the transformation of ferrihydrite to goethite.^{30–32} Thus, banded iron formations (BIFs) and other iron oxide-rich deposits can be U sinks and have been reported to harbor lighter U isotope signatures in comparison to that of contemporaneous seawater.^{15,25,33} The accumulation of lighter U isotopes in Mn/Fe oxides has been attributed, for example, to adsorption.^{34,35} Furthermore, while U(IV) species are major products of U(VI) reduction, there is increasing evidence for the presence of pentavalent U (U(V)).^{31,32,36,37} Our study³⁷ showed the occurrence of U(V) as a result of U(VI) reduction by preformed magnetite and its persistence prior to further reduction to form U(IV)O₂ nanoparticles. Furthermore, during the dissolution and recrystallization of Fe(II)-bearing minerals, the coprecipitation of U(VI) with magnetite and green rust, or the reduction of U(VI) incorporated in goethite, U(V) incorporation into the bulk mineral or near-surface structures is well documented, leading to the persistence of U(V) as uranate(V).^{31,32,36,38} The isotope fractionation imparted upon U during these processes remains unexplored as does the stability of the U isotope signature in the mineral matrix. Investigation of the U(V) isotope signature and its dynamics is needed to advance our understanding of the fundamentals of uranium isotope fractionation, to refine interpretation of the origin of light or heavy U isotope signature in modern and paleo-sediments, and to constrain the application of U isotopes to groundwater remediation.

The major goals of this study are to decipher the isotopic signature of U preserved as U(V) in an iron oxide matrix and to determine its stability to environmental conditions. Iron oxide surface-associated U can be desorbed, dissolved, or reoxidized.³⁹ As a result, only mineral matrix-associated U may remain as long as the iron oxide itself does not undergo alteration. This fact underscores the importance of investigating the persistence and the isotope signatures of iron oxide matrix-associated U, particularly for paleo-redox applications.

We tackle the specific case of U incorporated in magnetite, a common mineral in reducing environments. U(VI) was coprecipitated with magnetite under anoxic conditions, resulting in the incorporation of U(V) in the mineral. A series of wet chemistry treatments followed to retain only U(V). The stability of the isotopic signature of the incorporated U was monitored upon exposure to air or to an isotopically heavy U(VI) solution. This work enhances our understanding of the behavior of U isotopes in soils, sediments, and rocks and facilitates the interpretation of U isotope signatures in iron-rich rocks in paleo-environments and modern environments.

■ MATERIALS AND METHODS

Sample Preparation. All experiments were performed in an anoxic chamber (MBraun) with an N₂ atmosphere and O₂ < 0.1 ppm. All reagents and chemicals were of ACS or optimal grade (hydrochloric acid). Aqueous solutions were prepared with 18.2 MΩ cm water and were deoxygenated by N₂ purging prior to transfer into the anoxic chamber. All glassware and stoppers were cleaned with optimal grade 6 N HCl, rinsed with 18.2 MΩ cm water, and dried before usage.

U-magnetite nanoparticles were synthesized by coprecipitation.³¹ Briefly, anoxic solutions of 0.1 M FeCl₃ (40 mL), 0.1 M FeCl₂ (20 mL), and 20 mM uranyl chloride (1 mL, IRMM184, stored in 0.1 N isotope grade HCl) were mixed and continuously stirred inside the anoxic chamber. The pH of the mixture was increased by gradually adding 0.5 M NaOH until the pH value reached 7.8 ± 0.1 . The final total Fe concentration was 60 mM, while that of U(VI) was 200 μM. The as-synthesized U-magnetite coprecipitate suspension (abbreviated as *U-mag*) contained a magnetite concentration of 4.64 g magnetite/L (equivalent to an Fe aqueous concentration of 60 mM) and a final U concentration of 4.3×10^{-5} mol/g magnetite (equivalent to an aqueous concentration of $\sim 203 \mu\text{M}$) and was sealed in a serum bottle. After 12 h, the pH value was readjusted to 7.8 ± 0.1 if necessary. Replicate coprecipitated *U-mag* suspensions were

Table 1. Fraction of U(IV), U(V), and U(VI) Components in Each U-Bearing Magnetite Solid Sample as Calculated by the Iterative Transformation Factor Analysis (ITFA) method^{50a}

composition (%)	U(IV) (%)	U(V) (%)	U(VI) (%)	composition (%)	U(IV) (%)	<i>U-mag-HCl-2</i> (%)	U(VI) (%)
<i>U-mag</i>	16 ± 1	78 ± 2	6 ± 2	<i>U-mag-doped</i>	45 ± 1	55 ± 2	-
<i>U-mag-bic</i>	15 ± 1	83 ± 2	2 ± 2	<i>U-mag-doped-HCl</i>	-	97 ± 2	3 ± 2
<i>U-mag-HCl</i>	-	96 ± 2	4 ± 2	<i>U-mag-oxidized</i>	-	67 ± 2	33 ± 2
<i>U-mag-HCl-2</i>	-	94 ± 2	6 ± 2	<i>U-mag-oxidized-HCl</i>	-	84 ± 2	16 ± 2

^a*U-mag-doped*, *U-mag-doped-HCl*, *U-mag-oxidized*, and *U-mag-oxidized-HCl* were collected after 2 months of incubation. On the left-hand-side table, the composition of *U-mag* solids is shown as a function of UO₂(U(IV)), BiUO₄(U(V)), and uranyl-acetate (U(VI)). The corresponding estimated root-mean-square error (RMS) associated with the ITFA analysis³¹ were reported as 1% for U(IV) and 2% for U(V) and U(VI), representing the relative error. On the right-hand-side table, the composition of treated *U-mag* solids is shown as a function of the U(IV) and U(VI) references as well as the *U-mag-HCl-2* (a replicate sample to *U-mag-HCl*) solid shown on the left-hand-side table to be composed mostly (94%) of U(V) with the corresponding RMS <1% for U(IV) and 2% for U(V) and U(VI). -bic represents bicarbonate treatment.

stored in sealed serum bottles in the anoxic chamber for 10 days prior to further treatment. XRD spectra of the U-containing magnetite solids are available (Figure S1). Please note that solid-phase names are italicized throughout this article.

The isotope signatures measured for all samples are reported in the delta notation ($\delta^{238}\text{U}$) relative to the IRMM184 stock (eq 1) to indicate the direction and extent of isotope fractionation by comparing the measured U isotope signature to the initial signature (IRMM-184) before experiments. Thus, the initial solution uranyl chloride carries an isotope signature of $\delta^{238}\text{U} = 0\text{‰}$

$$\delta^{238}\text{U} = \left[\frac{(^{238}\text{U}/^{235}\text{U})_{\text{sample}}}{(^{238}\text{U}/^{235}\text{U})_{\text{IRMM184}}} - 1 \right] \times 1000[\text{‰}] \quad (1)$$

Isotope Exchange. Isotope exchange experiments were performed to investigate the stability of the U isotope signature present within the iron oxide structure. The originally synthesized *U-mag* suspension was aged inside the anoxic chamber for a year (*U-mag-aged*). In parallel, the original *U-mag* suspension was mixed with a freshly prepared uranyl(VI)-chloride solution with a $\delta^{238}\text{U} = 4.5\text{‰}$ containing 5 mM bicarbonate, which was prepared by mixing depleted uranium as U(VI)-chloride ($^{238}\text{U}/^{235}\text{U} = \sim 499$) with the IRMM184 uranyl(VI)-chloride stock solution ($^{238}\text{U}/^{235}\text{U} = 137.68$).⁴⁰ The newly prepared suspension (1.16 g magnetite/L) was abbreviated as *U-mag-doped* (8.6×10^{-5} mol of U/g magnetite, equivalent to $\sim 100 \mu\text{M}$ of aqueous U) (Figure 1) and included $\sim 50\%$ of U from the *U-mag* suspension and $\sim 50\%$ from the newly introduced heavy isotope-doped U(VI) solution (replicate 1, 50% *U-mag* and replicate 2, 55% *U-mag*). Additionally, 50 mL of the original *U-mag* suspension (4.64 g magnetite/L, containing 203 μM U) was removed from the anoxic chamber and placed under ambient conditions (open to the atmosphere) to undergo oxidation. This treatment is referred to as *U-mag-oxidized* (Figure 1). The *U-mag-doped* and *U-mag-oxidized* suspensions were monitored over time and probed at 0.5, 1, 2, 4, and 6 months for changes in the U isotope signature. Figure 1 offers a schematic of the experimental design.

U Species Separation. A bicarbonate extraction (100 mM) was applied to three of the four types of solid phases (*U-mag*, *U-mag-doped*, and *U-mag-oxidized*) in order to extract surface-associated U(VI) species by the formation of soluble uranyl-carbonate complexes.⁴¹ After equilibrating 5 mL of each type of suspension with 5 mL of 200 mM bicarbonate solution for 30 min (final concentration 100 mM), the

remaining solid phase and the extracted aqueous-phase solution were separated with a strong Nd magnet. The remaining solids were collected as *U-mag-bic*, *U-mag-doped-bic*, and *U-mag-oxidized-bic*, corresponding to the bicarbonate extraction. The results of extraction with a 50 mM bicarbonate solution are presented in Table S1. Alternatively, HCl solutions (2–2.5 mM HCl final concentration) were applied to induce the dissolution of insoluble uraninite from the magnetite surface. The 2.5 mM HCl solution induced the release of U into solution while affecting minimal magnetite dissolution (Table S2). A higher concentration of HCl (2.8 mM HCl) was used for extraction of the *U-mag-doped* suspension due to the higher pH value of this system. Similar to the bicarbonate treatment, the magnetite suspension was equilibrated with HCl for 30 min, and the remaining solids were collected magnetically as *U-mag-HCl*, *U-mag-doped-HCl*, and *U-mag-oxidized-HCl*. For both types of extractions, the aqueous phase remaining after Nd magnet separation was filtered through a PTFE filter (0.22 μm) to remove any particles remaining in the supernatant. The amount of U collected on the filter was negligible (as determined by digestion with 6 N HCl), and thus, its isotope composition could not be measured. The concentration of U was measured in the extracted aqueous phase as well as in the collected solid (after complete digestion with 6 N HCl). Only part of the solid sample was digested for isotope measurements because most of it was used for synchrotron-based characterization (see below). The percentage of U in the solid phase was thus calculated based on the measured extracted aqueous U and the total U concentrations. All extraction procedures were performed in the anoxic chamber, except the treatment of *U-mag-oxidized* samples. Bicarbonate extraction and acid leaching have been reported not to induce U isotope fractionation.^{25,28}

Aqueous Phase and Isotope Analysis. Aqueous-phase solutions and digested solid solutions were diluted with 1% HNO₃ to appropriate concentrations for U and Fe measurements by inductively coupled plasma–mass spectrometry (ICP-MS, PerkinElmer). Samples were stored and shipped in Falcon tubes to Hannover in Germany for U isotope measurements. Samples were prepared for measurements of isotopic composition on a Thermo Scientific-Neptune multi-collector inductively coupled plasma source mass spectrometer (MC-ICP-MS), as previously.^{42,43} More detail is provided in Text S1.

Solid Characterization. The uranium valence state was determined in solid phases using X-ray absorption near-edge structure (XANES) spectroscopy at the M₄-edge (3725 eV) with high-energy-resolution fluorescence detection (HERFD).

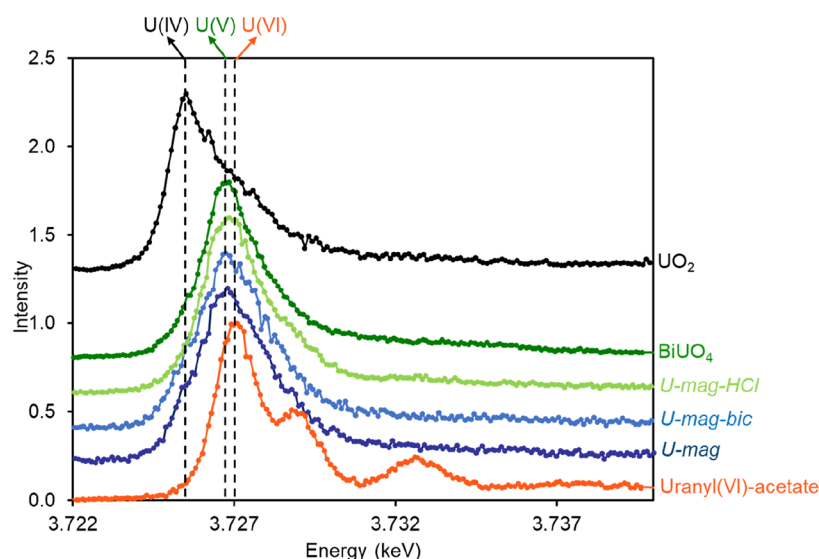


Figure 2. U M_4 -edge HERFD-XANES spectra for the original *U-mag* for the remaining solid phase after extracting *U-mag* with bicarbonate solution (*U-mag-bic*) and for the remaining solid phase after extracting *U-mag* with 2.5 mM HCl (*U-mag-HCl*). For comparison, $U(IV)O_2$, $BiUO_4$ ⁵¹ (uranate U(V)), and uranyl(VI)-acetate reference spectra are included. Dashed lines indicate the white line energy position for U(IV), U(V), and U(VI) valence states. The $BiUO_4$ spectrum is the same as that reported by Popa et al.⁵¹

This measurement was performed using a Johann-type X-ray spectrometer^{44–46} installed at the ACT endstation of the CAT-ACT-Beamline for catalysis and actinide/radionuclide science at the KIT synchrotron radiation facility, Karlsruhe.⁴⁷ Detailed descriptions on the sample preparation, the M_4 -edge HERFD-XANES measurement, and spectral analysis are included in Text S2. The U L_3 -edge X-ray adsorption spectroscopy measurements were performed at the Diamond Light Source, beamline I20-Scanning, and sample preparation and measurements were the same as those described in Pan et al.³⁷ Sample preparation for transmission electron microscopy (TEM) analysis is also described in Text S3.

RESULTS AND DISCUSSION

Characterization of Reduction Products. *U-mag Coprecipitate.* Based on previous studies, the formation of U(V) was expected as the main product of U(VI) coprecipitation with magnetite.^{31,32} By comparison to the spectra of uraninite, $BiUO_4$, and uranyl acetate as references for U(IV), U(V), and U(VI), respectively, M_4 -edge HERFD-XANES spectra of the coprecipitated *U-mag* solid support the presence of $6 \pm 2\%$ U(VI), $78 \pm 2\%$ U(V), and $16 \pm 1\%$ U(IV) (Table 1 and Figure 2). Thus, a U(V) species was confirmed to be the dominant reduced product. The L_3 -edge XANES spectra also show the presence of mixed valence states. The broadness of the spectra at the energy position of the white line (Figure S2a) area suggests a typical uranate type of structure for U(V)/U(VI) species,^{31,48,49} indicating the incorporation of U into the magnetite structure. From Fourier transforms of the L_3 -edge EXAFS spectra, the distinct peak (Figure S2c) further confirms the presence of a U–Fe pair correlation, indicating the substitution of U for Fe atoms at octahedral sites.^{31,32} Thus, we propose that the coprecipitated *U-mag* solid is similar to that produced by others, and U(VI) and U(IV) remained on the magnetite surface, while the stabilization of U(V) was achieved by its incorporation into the magnetite structure.

Bicarbonate Extraction. Following coprecipitation of *U-mag*, wet chemistry treatments were applied aiming to separate

U species according to their valence state. Unreduced U(VI) adsorbed on the magnetite surface was removed with a 100 mM bicarbonate solution, releasing $\sim 1\%$ of the total U into the extracted aqueous phase (Table 2). Additionally, the M_4 -edge

Table 2. Fraction of U in the Solid and Aqueous Phases after Treatment of Duplicate U(VI)-Magnetite Coprecipitated Solids (*U-mag*) with Either a Bicarbonate or an HCl Solution and the Corresponding Individual Isotope Signatures in Either the Extracted Aqueous Phase or the Remaining Solid Phase^a

	<i>U-mag</i> replicate 1		<i>U-mag</i> replicate 2	
	% of U	$\delta^{238}U$ ‰	% of U	$\delta^{238}U$ ‰
100 mM Bicarbonate Extraction				
aqueous (<i>U-mag-bic-aq</i>)	1.2%	-0.68 ± 0.01	0.8%	-0.89 ± 0.04
solid (<i>U-mag-bic</i>)	98.8%	-	99.2%	0.02 ± 0.01
2.5 mM HCl Extraction				
aqueous (<i>U-mag-HCl-aq</i>)	17.7%	0.34 ± 0.01	18.9%	0.30 ± 0.06
solid (<i>U-mag-HCl</i>)	82.3%	-0.11 ± 0.06	81.1%	-0.13 ± 0.01

^aA dash indicates that data were not collected. -bic represents bicarbonate treatment.

HERFD-XANES spectrum of the remaining solid phase (*U-mag-bic*) was interpreted by ITFA analysis⁵⁰ and showed a decrease in the contribution of U(VI) species, confirming that the majority of U(VI) was successfully removed (Table 1 and Figure 2). Thus, the U species in the extracted solution (*U-mag-bic-aq*) were considered to represent U(VI) for the purposes of isotopic analysis. The removal of U(VI) only resulted in a slight increase of the fraction of U(V) but not in that of U(IV) (Table 1), likely due to the limitations of synchrotron measurements ($\sim 8\%$ error as the relative error) and the error associated with ITFA analysis. Incidentally, LCF analysis with Athena yields similar results (Table S3).

HCl Extraction. Based on the XANES analysis, there is a $16 \pm 1\%$ contribution of U(IV) in *U-mag*. Considering previous work,³¹ U(IV) is most likely present as uraninite (UO₂) at the magnetite surface. Thus, obtaining a U(V)-only sample from *U-mag* requires the removal of UO₂. HCl solutions of increasing concentration (1.5, 2, and 2.5 mM) were applied individually, aiming to dissolve UO₂ while minimizing the dissolution of magnetite and the release of incorporated U species. With 1.5 and 2 mM HCl, only between 0.3 and 2% of the total U was extracted, with 6–8% of the total Fe released into the extracted solutions, suggesting that the HCl concentration was too low to achieve sufficient uraninite dissolution (Table S2). After extracting *U-mag* with 2.5 mM HCl for 30 min, a large amount of U (~18% of total U) and Fe (~10% of total Fe) were extracted. The amount of U extracted (~18%) is comparable to the sum of the fractions of U(VI) and U(IV) (~22%) detected in *U-mag* by M₄-edge HERFD–XANES (Table 1). The M₄-edge HERFD–XANES spectrum of *U-mag-HCl* showed a significant intensity decrease at the energy position corresponding to U(IV) species (Figure 2), suggesting the successful removal of the majority of U(IV). ITFA confirmed that $96 \pm 2\%$ of U in *U-mag-HCl* was in the pentavalent valence state (Table 1). Thus, a nearly pure U(V) solid phase was obtained, while most of the U(IV) species was dissolved in the HCl extracted solution. It also confirms that in the *U-mag* sample, most of the U(IV) was present at the magnetite surface. Fe detected in the 2.5 mM HCl solution (corresponding to ~10% of total Fe) suggests that the dissolution of some magnetite solid occurred, and thus, the release of incorporated U(V) into the extracted phase cannot be ruled out. However, the fact that the U(IV) signal nearly disappeared in the M₄-edge HERFD–XANES suggests that a major part of the U released originated from U(IV) (at the surface) rather than U(V) incorporated in iron oxide. This is because the amount of U removed by HCl treatment (17.7%) corresponded to the percentage of U(IV) in the *U-mag* solid phase ($16 \pm 1\%$). Thus, the U species in the extracted solution should be dominated by U(IV), while a small amount of U(VI) and U(V) is present. As the two Fe valence states are expected to be released from magnetite dissolution, uranate(V) could undergo (1) disproportionation into U(IV) and U(VI), (2) reoxidation to U(VI) by aqueous Fe(III), or (3) reduction to U(IV) with aqueous Fe(II). The accurate quantification of the aqueous fractions of U(IV), U(V), or U(VI) and the corresponding isotope signatures would require further studies. We consider the U species in the aqueous phase resulting from HCl treatment as an overall HCl-extractable form that includes mostly U(IV).

U(V) Isotopic Signature. Based on the solid-phase characterization, we confirmed the formation and stabilization of magnetite-associated U(V) species, preventing either reduction to U(IV) or disproportionation to U(IV) and U(VI) under anoxic conditions. The removal of U(VI) and U(IV) species at the magnetite surface through extractions provided the opportunity to identify the U(V) isotopic signature. Through bicarbonate extraction, the U(VI) adsorbed on the magnetite surface was extracted into sample *U-mag-bic-aq* and the corresponding $\delta^{238}\text{U}$ value ranged from -0.89 to -0.68% . This finding suggests the preferential reduction of heavy U(VI) to U(V) or U(IV). Thus, the light isotope accumulates in the remaining U(VI) species.

Through HCl extraction, the majority of U(IV) and U(VI) species were removed. Although the composition of U(VI)/

U(V)/U(IV) in the extracted solution is not resolvable, the remaining solid phase (*U-mag-HCl*) was confirmed to consist mainly of U(V) species with a $\delta^{238}\text{U}$ value of -0.11 or -0.13% , demonstrating that U(V) carries a slightly light isotope signature but heavier than U(VI). This is the first elucidation of the isotope signature of U(V) species.

As both U(VI) and U(V) exhibit light isotope signatures, the heavy isotope must accumulate in the U(IV) species. The majority of U(IV) was successfully extracted by the 2.5 mM HCl solution. The associated $\delta^{238}\text{U}$ in the extracted solution was 0.34 or 0.30‰ (from replicate *U-mag* suspensions). A small amount of U(VI) and U(V) surely contributed to the overall isotope signature of the extracted aqueous phase, suggesting that the $\delta^{238}\text{U}$ of the pure U(IV) species should be slightly more positive than the values above. In fact, assuming that only U(IV) and U(VI) species were present in the HCl-extracted aqueous phase and that 1.2% of U(VI) was released in *U-mag-HCl-aq* (as it was in *U-mag-bic-aq*), then the remaining U(IV) would carry an isotope signature of $0.41 \pm 0.01\%$ (calculation in the Supporting Information, Text S4). Comparison of the weighted sum of $\delta^{238}\text{U}$ values for U in the extracted solutions ($\delta^{238}\text{U} = 0.34\%$ for 17.7% of U in *U-mag-HCl-aq*) and that in the remaining solid phase ($\delta^{238}\text{U} = -0.11\%$ for 82.3% of the U in *U-mag-HCl*) evidenced a difference of only $\delta^{238}\text{U} = -0.03\%$ relative to the starting solution, demonstrating isotope mass balance for this system.

Thus, we characterized the isotopic fractionation associated with the incorporation of U species into the iron oxide structure and the one-electron transfer during the abiotic reductive coprecipitation of U(VI). Although a precise isotopic signature could not be determined for U(IV), the direction of isotope fractionation during U(VI) incorporation into the iron oxide structure and reduction to U(IV) was identified as $\delta^{238}\text{U}_{\text{U(VI)}} < \delta^{238}\text{U}_{\text{U(V)}} < \delta^{238}\text{U}_{\text{U(IV)}}$. The accumulation of the heavy isotope in U(IV) and the light isotope in U(VI) and U(V) conforms to the valence-dependent trend predicted by NFS-dominated equilibrium isotope fractionation and provides a reduction mechanism that may explain lighter solid-phase isotope signatures observed in the iron-rich rocks or sediments.

Stability of the U Isotopic Signature in Magnetite.

While U oxidation, desorption, complexation, or reduction may alter the isotope composition of the U species associated with the mineral surface, stably mineral-incorporated U can provide more robust insight into the isotopic signature of U that persists regardless of the chemical environment. A previous study has reported the persistence of incorporated U(V) when coprecipitated U(V)-containing magnetite was exposed to O₂ for 1 year, suggesting the stability of incorporated U(V).³¹ However, over long-term laboratory studies, atomic exchange of Fe atoms between the solid phase and surface or solution could occur^{52–54} and may affect the stability of U valence states and their isotopic signature. Thus, we investigated the stability of the isotopic signature of U species incorporated within the magnetite structure in *U-mag* in two ways. One was by equilibrating the *U-mag* suspension with a heavy isotope-doped U(VI)-carbonate solution under anoxic conditions. This treatment was intended to represent the exchange between U(V) incorporated in magnetite and solution U(VI) under anoxic conditions. The second was by exposing the *U-mag* suspension to the atmosphere. This treatment was intended to represent exposure of U(V)-doped magnetite to oxic conditions. As a control, the *U-mag*

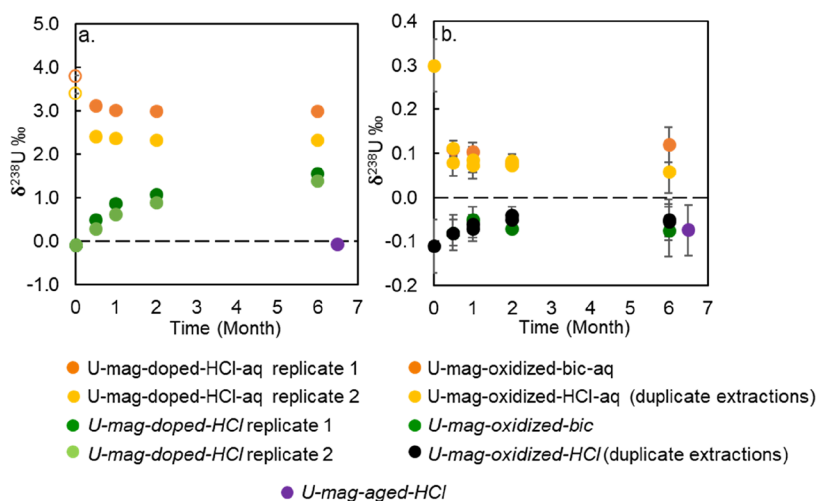


Figure 3. Isotope signatures of U in the HCl-extracted aqueous phase and remaining in the solid phase for (a) *U-mag-doped* and (b) *U-mag-oxidized*. (a) Orange and yellow symbols: isotopic signature of U in the HCl-extracted aqueous phase in duplicate *U-mag-doped* reactors; the unfilled symbols represent the calculated $\delta^{238}\text{U}$ of the initial HCl-extracted phase for replicates; dark green and light green symbols: isotopic signature of U remaining in the solid phase after HCl extraction in duplicate *U-mag-doped* reactors. (b) Orange and yellow symbols: isotopic signature of U in the bicarbonate-extracted and HCl-extracted (duplicate extractions) aqueous phase for *U-mag-oxidized*; dark green and black symbols: isotopic signature of U in *U-mag-oxidized-bic* (only one extraction) and *U-mag-oxidized-HCl* (duplicate extractions) samples, respectively. The purple symbol in (a,b): isotopic signature of U in the *U-mag-aged-HCl* sample. Error bars represent measurement 2 S.D. values. In (a), the 2 S.D. values were smaller ($<0.1\text{‰}$) than the marker.

suspension (replicate 1) was stored for 1 year under anoxic conditions, producing a *U-mag-aged* suspension.

First, we consider the control *U-mag-aged* and produce a HCl-extracted solid phase (*U-mag-aged-HCl*) through treatment with 2.5 mM HCl ($\sim 20\%$ of U was extracted) (Figure 1). The $\delta^{238}\text{U}$ value associated with U in the remaining solid after HCl extraction was $-0.07 \pm 0.06\text{‰}$, which was undistinguishable from the $\delta^{238}\text{U}$ value for the original *U-mag-HCl* sample of $-0.11 \pm 0.06\text{‰}$. The result suggests the stability of the isotopic signature of the U(V) species incorporated within the magnetite structure under long-term and constant laboratory conditions, such as those that could be encountered post-remediation.

U-mag Amended with Heavy U(VI). The *U-mag-doped* suspension extracted with a bicarbonate solution showed that the amount of bicarbonate-extractable U (i.e., U(VI)) decreased over time from 17 to 10%, then 2%, and finally $<1\%$ (Figure S3a). This result evidences the reduction of the amended heavy U(VI) carbonate by magnetite in *U-mag* (Figure S3a). In contrast, HCl extractions (2.8 mM HCl) removed a similar amount of U ($\sim 60\%$) from *U-mag-doped* samples at all time points with $\sim 40\%$ of the total U remaining in the solid (as *U-mag-doped-HCl*). In the *U-mag* sample, about 80% of the total U was incorporated within the magnetite structure as U(V). However, the addition of heavy U(VI) to *U-mag* doubled the overall amount of U in the system. Thus, it is expected, and observed, that if incorporated U(V) remains within magnetite, it would represent about 40% of total U in the *U-mag-doped* sample. In order to ascertain the valence state of U within the solid-phase matrix in the *U-mag-doped* sample, we compared their $M_{4,5}$ -edge HERFD–XANES spectra to those of two replicate *U-mag-HCl* samples (*U-mag-HCl* and *U-mag-HCl-2*, corresponding to replicate *U-mag* batches). We previously established that *U-mag-HCl* was composed of mostly U(V) (Table 1 and Figure S4). As expected, *U-mag-doped* was composed of 45% U(IV), while 55% of U corresponded to *U-mag-HCl-2* (i.e., U(V)), which corresponds

to the same original batch of *U-mag*. This finding confirms that heavy U(VI) amended to *U-mag* was reduced to U(IV). In the *U-mag-doped-HCl* sample, U(IV) was no longer detected and the U speciation consisted of 97% U(V) and 3% U(VI). This result demonstrates that the amendment of additional U(VI) did not alter the speciation of the U incorporated in magnetite.

U isotope signatures in the HCl-extracted solution (*U-mag-doped-HCl-aq*) and remaining solids (*U-mag-doped-HCl*) were measured. $\delta^{238}\text{U}$ of the extracted aqueous phase decreased from ~ 3.8 to 3.00‰ (and 3.4 to 2.33‰ for the replicate) and that in the solid phase increased from -0.1 to $\sim 1.5\text{‰}$ (Figure 3a and Table S4). It should be noted that the $\delta^{238}\text{U}$ values of 3.8 and 3.4‰ were calculated as HCl extraction was not performed immediately after the preparation of *U-mag-doped* samples (Table S4). Based on the HCl extraction results and the XANES measurements, it appears that heavy U(VI) amended to the *U-mag* suspension was readily reduced to U(IV) at the magnetite surface (as it was readily extractable by HCl treatment). However, as observed, the U isotope signature in the remaining solid phase increased from -0.1 to 1.5‰ , suggesting that either the U species with a heavy isotope was incorporated into the magnetite phase or U(IV) was not completely removed by the HCl extraction. To identify the most likely explanation, we calculated the percentage of heavy U(IV) that must remain after HCl extraction to account for the measured increase in $\delta^{238}\text{U}$ in the solid phase. For instance, at 2 months, a contribution of at least 25% of U(IV) (assuming that all newly formed U(IV) has the highest $\delta^{238}\text{U}$ of 4.5‰) is needed to account for the observed 1.1‰ increase in $\delta^{238}\text{U}$ in *U-mag-doped-HCl* (replicate 1). However, U(IV) was not detected by XANES in the 2 month *U-mag-doped-HCl* sample and would have been had it accounted for 25% of the total U. Thus, this result indicates that the increase in $\delta^{238}\text{U}$ values is likely due to the incorporation of heavy U(V) in magnetite.

Considering the extracted U, the fraction of U extracted with HCl does not vary over time (Figure S3a), while the

corresponding $\delta^{238}\text{U}$ in the extracted aqueous phase decreases over time (Figure 3a). This trend indicates the release of incorporated U(V), carrying a slightly light isotope signature, into the extracted aqueous phase.

On one hand, we observe only small changes in the amount of U incorporated in magnetite over time and that its valence state remains pentavalent. On the other hand, we observe a trend in the isotope signature pointing to the incorporation of heavy U into magnetite and the release of lighter U into the solution. We conclude that together, these observations point to iron mineral dynamics, where dissolution and recrystallization and additional U(V) incorporation might occur. The dynamics of the mineral phase is particularly evident when contrasted with the *U-mag-aged-HCl* sample that exhibited the same isotopic signature as the initial sample after 1 year of equilibration. We attribute the difference in the behavior of the two systems to the introduction of U(VI)-chloride and bicarbonate, which (1) altered the water chemistry as the pH increased from 7.8 to 8.2 due to the presence of 5 mM bicarbonate in solution and (2) induced the reduction of additional U(VI) on the surface and the associated oxidation of Fe(II) in magnetite particles. We hypothesize that the pH change and the redox equilibration were sufficient to affect dissolution and reprecipitation of magnetite, allowing for an exchange between U on the magnetite surface and U incorporated within magnetite.

U-mag Equilibrated with Air. After equilibration with air for 0.5, 1, 2, or 6 months, treatment of the suspension with either bicarbonate or HCl extracted a similar amount of U (~20%, Figure S3b), suggesting that the ~15% of the U(IV) in the original *U-mag* (Table 1) was oxidized to U(VI) and, consequently, was extractable by both bicarbonate and HCl solutions. M_4 -XANES analysis shows a contribution of $67 \pm 2\%$ U(V) and $33 \pm 2\%$ U(VI) in the *U-mag-oxidized* suspension (Table 1). Thus, the contribution of U(V) to the *U-mag-oxidized* suspension is lower than that prior to oxidation (because *U-mag* harbors $78 \pm 2\%$ U(V)). Furthermore, the contribution of U(VI) to *U-mag-oxidized* was greater than the sum of U(VI) and U(IV) in the *U-mag* sample. This suggests that both U(IV) and a part of U(V) were oxidized through exposure to air. Indeed, after HCl extraction, the M_4 -edge HERFD XANES spectra of *U-mag-oxidized-HCl* show the presence of a contribution of $16 \pm 2\%$ of U(VI) in addition to $84 \pm 2\%$ of the U species present in U(V). The data suggest that part of the incorporated U(V) was oxidized to U(VI). Most likely, the latter remained incorporated in the solid phase and was unextractable by HCl solution. The incorporation of U(VI) in iron oxide structures has been reported in the hematite structure.⁵⁵

In the *U-mag-oxidized* system, a decrease of $\delta^{238}\text{U}$ values in the extracted aqueous phase (*U-mag-oxidized-HCl-aq* or *U-mag-oxidized-bic-aq*) was only observed in the first 2 weeks (from 0.3 to 0.1‰), while the $\delta^{238}\text{U}$ in the solid phase (*U-mag-oxidized-HCl*) remained unchanged. Indeed, $\delta^{238}\text{U}$ varied from -0.11 ± 0.06 to -0.07 ± 0.06 ‰ in the *U-mag-oxidized-HCl* (black symbols in Figure 3b) or *U-mag-oxidized-bic* (dark-green symbols in Figure 3b) samples. These results point to the stable isotope signature of U incorporated within magnetite despite partial oxidation of U(V) to U(VI). We propose that the equilibration of the *U-mag* suspension with the atmosphere resulted in the rapid oxidation of the magnetite surface to maghemite until depletion of surface Fe(II). There is likely quantitative oxidation of U(V) in a near-surface layer, resulting

in no isotopic fractionation (as was shown for quantitative oxidation of U(IV) in uraninite).⁵⁶ The result of wet chemical treatment indicated that there was no significant change in the amount of U incorporated over time, and M_4 -edge HERFD-XANES analysis also suggested little change in the speciation of incorporated U species (except partial oxidation of U(V) to U(VI) in the *U-mag-oxidized* sample).

Comparison of the three systems, *U-mag-aged*, *U-mag-doped*, and *U-mag-oxidized*, reveals that dynamic isotope exchange occurs only when the chemical conditions change, likely requiring re-equilibration of the magnetite surface under distinct water chemistry conditions. When the chemistry of the system is unaltered, such as in the aged *U-mag*, the $\delta^{238}\text{U}$ in the HCl-extracted solid phase remains at a value of -0.07 ± 0.06 ‰, suggesting the stability of the U(V) isotope signature. Also, in the *U-mag-oxidized* system, a slight variation of $\delta^{238}\text{U}$ values was detected in the aqueous phase within the first 2 weeks, corresponding to the time during which the surface of magnetite was oxidized. After this point, surface Fe(II) was absent, and no further change in isotopic signature was observed. In contrast, when water chemistry conditions changed, particularly upon the introduction of a U(VI)-bicarbonate solution in the *U-mag-doped* system, mineral dynamics of magnetite was suggested. The oxidation of Fe(II) in the magnetite structure and the change of the pH value from 7.8 to ~8.2 might have induced the dissolution and reprecipitation of a small fraction of iron oxide with the presence of surface or aqueous Fe(II). Scherer's group has proposed the redox conveyor belt theory for iron oxide minerals (goethite and hematite) where spatially separated adsorption and release of Fe(II) at the mineral surface could occur, even though no visible dissolution and precipitation of iron oxide minerals were observed.^{53, 54} High-angle angular dark field (HAADF) STEM images of *U-mag*, *U-mag-HCl*, *U-mag-doped*, and *U-mag-oxidized* samples did not show obvious differences in magnetite morphology and particle size (Figure S5). Based on the fast Fourier transform (FFT) analysis, all the nanoparticles can still be fitted with the magnetite crystal structure using the JEMS software.⁵⁷ Even when the nanoparticles should have been partially oxidized to maghemite in the *U-mag-oxidized* sample, the differences between magnetite and maghemite could not be distinguished via FFT analysis. XRD spectra of *U-mag*, *U-mag-HCl*, and *U-mag-doped* samples also confirmed the magnetite phase (Figure S1). Although the tools used did not allow direct observation of mineral dynamics, it remains the most parsimonious explanation for the data collected.

Overall, the isotopic signature of pentavalent U(V) in magnetite is stable, except in the cases where mineral dynamics, which would result in the incorporation of U species originating outside the mineral phase, occurs. In this scenario, the isotope signature of the U species originally incorporated in the mineral structure is impacted by exchange with U on the magnetite surface.

ENVIRONMENTAL IMPLICATIONS

Monitoring the success of reductive remediation strategies to immobilize U *in situ* benefits from U isotope measurements. Additionally, the investigation of U isotope signatures in the geological rock record can advance the understanding of redox conditions in paleo-environments. Iron-rich rocks in BIF have been reported to exhibit either negative $\delta^{238}\text{U}$ values (as low as -0.9 ‰) or $\delta^{238}\text{U}$ values close to that of background igneous

rocks (−0.4 to −0.2‰).²⁵ The two major interpretations invoked to explain the solid-phase light isotope are the preferential adsorption of ²³⁵U onto mineral surfaces^{34,35} and the reduction of ²³⁵U by preformed magnetite.²⁸ However, U and Fe coprecipitation is also a scenario for uranium sequestration by iron oxides during the formation of BIF. During the sporadic increase of seawater oxygen level before the great oxygen event (i.e., whiffs of oxygen),⁵⁸ the oxidation of Fe(II) to Fe(III) and the coprecipitation of Fe(II) and Fe(III) with U(VI) might result in the sequestration of uranium(V) within iron oxides. These minerals, formed under anoxic conditions, may be transformed under oxic conditions (or vice versa), but pentavalent U would remain incorporated in the mineral phase, with its isotopic signature protected from isotopic exchange. Thus, the present study provides insights into reaction pathways that could explain the preferential accumulation of ²³⁵U within some iron oxide phases and iron-rich sediments.

■ ASSOCIATED CONTENT

SI Supporting Information

The Supporting Information is available free of charge at <https://pubs.acs.org/doi/10.1021/acs.est.1c06865>.

Experimental details for TEM sample preparation and M₄-edge HERFD–XANES measurements and additional results and analysis for chemical extractions, XRD spectra, M₄-edge HERFD–XANES spectra, L₃-edge XANES spectra, and HAADF STEM images (PDF)

■ AUTHOR INFORMATION

Corresponding Author

Rizlan Bernier-Latmani – Environmental Microbiology Laboratory, École Polytechnique Fédérale de Lausanne, Lausanne 1015, Switzerland; orcid.org/0000-0001-6547-722X; Email: rizlan.bernier-latmani@epfl.ch

Authors

Zezhen Pan – Department of Environmental Science and Engineering, Cluster of Interfacial Processes Against Pollution (CIPAP), Fudan University, Shanghai 200438, China; Environmental Microbiology Laboratory, École Polytechnique Fédérale de Lausanne, Lausanne 1015, Switzerland; orcid.org/0000-0003-1712-3149

Yvonne Roebbert – Leibniz, Universität Hannover, Institut für Mineralogie, D-30167 Hannover, Germany; orcid.org/0000-0001-6705-1361

Aaron Beck – Institute for Nuclear Waste Disposal (INE), Karlsruhe Institute of Technology, Karlsruhe 76021, Germany

Barbora Bartova – Environmental Microbiology Laboratory, École Polytechnique Fédérale de Lausanne, Lausanne 1015, Switzerland

Tonya Vitova – Institute for Nuclear Waste Disposal (INE), Karlsruhe Institute of Technology, Karlsruhe 76021, Germany; orcid.org/0000-0002-3117-7701

Stefan Weyer – Leibniz, Universität Hannover, Institut für Mineralogie, D-30167 Hannover, Germany

Complete contact information is available at: <https://pubs.acs.org/doi/10.1021/acs.est.1c06865>

Author Contributions

The manuscript was written through contributions from all authors. R.B.L. conceived the research. Z.P. performed all the experiments with support from Y.R. and S.W., conducted the U isotope measurement, B.B., performed the STEM analysis, and A.B. and T.V., assisted with the HERFD–XANES measurements. All authors gave their approval for the final version of the manuscript.

Funding

The work at EPFL was supported by the Swiss National Science Foundation Grant 200021E-164209 and the European Research Council Consolidator Grant 725675 (UNEARTH).

Notes

The authors declare no competing financial interest.

Data availability: All relevant data are available from the authors or within the Supporting Information files. All relevant data and images are available from a data repository as <https://doi.org/10.5281/zenodo.5535727>.

■ ACKNOWLEDGMENTS

We thank Luca Loreggian and Ashley Brown at EPFL for helpful instructions and discussions. We thank the Institute for Beam Physics and Technology for the operation of the storage ring of the KIT synchrotron radiation facility, the Karlsruhe Research Accelerator (KARA). We acknowledge Dr. Jörg Rothe, Dr. Kathy Dardenne, Jurij Galanzew, and Bianca Schacherl for help with the organization and running of synchrotron experiments. We acknowledge the Diamond Light Source for time on Beamline I20-Scanning (L₃-edge EXAFS measurements) under proposal SP17472 and thank the beamline scientist Shu Hayama for beamtime assistance. We appreciate the comments of Associate Editor David Waite and three anonymous reviewers that helped us improve the presentation and interpretation of our study.

■ REFERENCES

- (1) Landa, E. R. Uranium Mill Tailings: Nuclear Waste and Natural Laboratory for Geochemical and Radioecological Investigations. *J. Environ. Radioact.* **2004**, *77*, 1–27.
- (2) Maher, K.; Bargar, J. R.; Brown, G. E. Environmental Speciation of Actinides. *Inorg. Chem.* **2013**, *52*, 3510–3532.
- (3) Veeramani, H.; Scheinost, A. C.; Monsegue, N.; Qafoku, N. P.; Kukkadapu, R.; Newville, M.; Lanzirrotti, A.; Pruden, A.; Murayama, M.; Hochella, M. F. Abiotic Reductive Immobilization of U(VI) by Biogenic Mackinawite. *Environ. Sci. Technol.* **2013**, *47*, 2361–2369.
- (4) Hyun, S. P.; Davis, J. A.; Sun, K.; Hayes, K. F. Uranium(VI) Reduction by Iron(II) Monosulfide Mackinawite. *Environ. Sci. Technol.* **2012**, *46*, 3369–3376.
- (5) Latta, D. E.; Boyanov, M. I.; Kemner, K. M.; O’Loughlin, E. J.; Scherer, M. M. Abiotic Reduction of Uranium by Fe(II) in Soil. *Appl. Geochem.* **2012**, *27*, 1512–1524.
- (6) Wu, W.-M.; Carley, J.; Fienen, M.; Mehlhorn, T.; Lowe, K.; Nyman, J.; Luo, J.; Gentile, M. E.; Rajan, R.; Wagner, D.; Hickey, R. F.; Gu, B.; Watson, D.; Cirpka, O. A.; Kitanidis, P. K.; Jardine, P. M.; Criddle, C. S. Pilot-Scale in Situ Bioremediation of Uranium in a Highly Contaminated Aquifer. 1. Conditioning of a Treatment Zone. *Environ. Sci. Technol.* **2006**, *40*, 3978–3985.
- (7) Watson, D. B.; Wu, W.-M.; Mehlhorn, T.; Tang, G.; Earles, J.; Lowe, K.; Gihring, T. M.; Zhang, G.; Phillips, J.; Boyanov, M. I.; Spalding, B. P.; Schadt, C.; Kemner, K. M.; Criddle, C. S.; Jardine, P. M.; Brooks, S. C. In Situ Bioremediation of Uranium with Emulsified Vegetable Oil as the Electron Donor. *Environ. Sci. Technol.* **2013**, *47*, 6440–6448.
- (8) Bopp, C. J.; Lundstrom, C. C.; Johnson, T. M.; Sanford, R. A.; Long, P. E.; Williams, K. H. Uranium 238U/235U Isotope Ratios as

Indicators of Reduction: Results from an in Situ Biostimulation Experiment at Rifle, Colorado, U.S.A. *Environ. Sci. Technol.* **2010**, *44*, 5927–5933.

(9) Shiel, A. E.; Johnson, T. M.; Lundstrom, C. C.; Laubach, P. G.; Long, P. E.; Williams, K. H. Reactive Transport of Uranium in a Groundwater Bioreduction Study: Insights from High-Temporal Resolution 238U/235U Data. *Geochim. Cosmochim. Acta* **2016**, *187*, 218–236.

(10) Schauble, E. A. Role of Nuclear Volume in Driving Equilibrium Stable Isotope Fractionation of Mercury, Thallium, and Other Very Heavy Elements. *Geochim. Cosmochim. Acta* **2007**, *71*, 2170–2189.

(11) Bigeleisen, J. Temperature Dependence of the Isotope Chemistry of the Heavy Elements. *Proc. Natl. Acad. Sci. U.S.A.* **1996**, *93*, 9393–9396.

(12) Fujii, Y.; Higuchi, N.; Haruno, Y.; Nomura, M.; Suzuki, T. Temperature Dependence of Isotope Effects in Uranium Chemical Exchange Reactions. *J. Nucl. Sci. Technol.* **2006**, *43*, 400–406.

(13) Rolison, J. M.; Stirling, C. H.; Middag, R.; Rijkbergen, M. J. A. Uranium Stable Isotope Fractionation in the Black Sea: Modern Calibration of the 238U/235U Paleo-Redox Proxy. *Geochim. Cosmochim. Acta* **2017**, *203*, 69–88.

(14) Brennecka, G. A.; Borg, L. E.; Hutcheon, I. D.; Sharp, M. A.; Anbar, A. D. Natural Variations in Uranium Isotope Ratios of Uranium Ore Concentrates: Understanding the 238U/235U Fractionation Mechanism. *Earth Planet. Sci. Lett.* **2010**, *291*, 228–233.

(15) Weyer, S.; Anbar, A. D.; Gerdes, A.; Gordon, G. W.; Algeo, T. J.; Boyle, E. A. Natural Fractionation of 238U/235U. *Geochim. Cosmochim. Acta* **2008**, *72*, 345–359.

(16) Montoya-Pino, C.; Weyer, S.; Anbar, A. D.; Pross, J.; Oschmann, W.; van de Schootbrugge, B.; Arz, H. W. Global Enhancement of Ocean Anoxia during Oceanic Anoxic Event 2: A Quantitative Approach Using U Isotopes. *Geology* **2010**, *38*, 315–318.

(17) Andersen, M. B.; Romaniello, S.; Vance, D.; Little, S. H.; Herdman, R.; Lyons, T. W. A Modern Framework for the Interpretation of 238U/235U in Studies of Ancient Ocean Redox. *Earth Planet. Sci. Lett.* **2014**, *400*, 184–194.

(18) Brüske, A.; Weyer, S.; Zhao, M.-Y.; Planavsky, N. J.; Wegwerth, A.; Neubert, N.; Dellwig, O.; Lau, K. V.; Lyons, T. W. Correlated Molybdenum and Uranium Isotope Signatures in Modern Anoxic Sediments: Implications for Their Use as Paleo-Redox Proxy. *Geochim. Cosmochim. Acta* **2020**, *270*, 449–474.

(19) Kendall, B.; Brennecka, G. A.; Weyer, S.; Anbar, A. D. Uranium Isotope Fractionation Suggests Oxidative Uranium Mobilization at 2.50Ga. *Chem. Geol.* **2013**, *362*, 105–114.

(20) Asael, D.; Tissot, F. L. H.; Reinhard, C. T.; Rouxel, O.; Dauphas, N.; Lyons, T. W.; Ponzevera, E.; Liorzou, C.; Chéron, S. Coupled Molybdenum, Iron and Uranium Stable Isotopes as Oceanic Paleoredox Proxies during the Paleoproterozoic Shunga Event. *Chem. Geol.* **2013**, *362*, 193–210.

(21) Zhang, F.; Lenton, T. M.; del Rey, Á.; Romaniello, S. J.; Chen, X.; Planavsky, N. J.; Clarkon, M. O.; Dahl, T. W.; Lau, K. V.; Wang, W.; Li, Z.; Zhao, M.; Isson, T.; Algeo, T. J.; Anbar, A. D. Uranium Isotopes in Marine Carbonates as a Global Ocean Paleoredox Proxy: A Critical Review. *Geochim. Cosmochim. Acta* **2020**, *287*, 27–49.

(22) Brennecka, G. A.; Herrmann, A. D.; Algeo, T. J.; Anbar, A. D. Rapid Expansion of Oceanic Anoxia Immediately before the End-Permian Mass Extinction. *Proc. Natl. Acad. Sci. U.S.A.* **2011**, *108*, 17631–17634.

(23) Holmden, C.; Amini, M.; Francois, R. Uranium Isotope Fractionation in Saanich Inlet: A Modern Analog Study of a Paleoredox Tracer. *Geochim. Cosmochim. Acta* **2015**, *153*, 202–215.

(24) Romaniello, S. J.; Herrmann, A. D.; Anbar, A. D. Uranium Concentrations and 238U/235U Isotope Ratios in Modern Carbonates from the Bahamas: Assessing a Novel Paleoredox Proxy. *Chem. Geol.* **2013**, *362*, 305–316.

(25) Wang, X.; Planavsky, N. J.; Hofmann, A.; Saupe, E. E.; De Corte, B. P.; Philippot, P.; LaLonde, S. V.; Jemison, N. E.; Zou, H.; Ossa, F. O.; Rybacki, K.; Alfimova, N.; Larson, M. J.; Tsikos, H.; Fralick, P. W.; Johnson, T. M.; Knudsen, A. C.; Reinhard, C. T.;

Konhauser, K. O. A Mesoarchean Shift in Uranium Isotope Systematics. *Geochim. Cosmochim. Acta* **2018**, *238*, 438–452.

(26) Basu, A.; Sanford, R. A.; Johnson, T. M.; Lundstrom, C. C.; Löffler, F. E. Uranium Isotopic Fractionation Factors during U(VI) Reduction by Bacterial Isolates. *Geochim. Cosmochim. Acta* **2014**, *136*, 100–113.

(27) Basu, A.; Brown, S. T.; Christensen, J. N.; Depaolo, D. J.; Reimus, P. W.; Heikoop, J. M.; Woldegabriel, G.; Simmons, A. M.; House, B. M.; Hartmann, M.; Maher, K. Isotopic and Geochemical Tracers for U(VI) Reduction and U Mobility at an in Situ Recovery U Mine. *Environ. Sci. Technol.* **2015**, *49*, 5939–5947.

(28) Stylo, M.; Neubert, N.; Wang, Y.; Monga, N.; Romaniello, S. J.; Weyer, S.; Bernier-Latmani, R. Uranium Isotopes Fingerprint Biotic Reduction. *Proc. Natl. Acad. Sci. U.S.A.* **2015**, *112*, S619–S624.

(29) Stirling, C. H.; Andersen, M. B.; Warthmann, R.; Halliday, A. N. Isotope Fractionation of 238U and 235U during Biologically-Mediated Uranium Reduction. *Geochim. Cosmochim. Acta* **2015**, *163*, 200–218.

(30) Massey, M. S.; Lezama-Pacheco, J. S.; Jones, M. E.; Ilton, E. S.; Cerrato, J. M.; Bargar, J. R.; Fendorf, S. Competing Retention Pathways of Uranium upon Reaction with Fe(II). *Geochim. Cosmochim. Acta* **2014**, *142*, 166–185.

(31) Pidchenko, I.; Kvashnina, K. O.; Yokosawa, T.; Finck, N.; Bahl, S.; Schild, D.; Polly, R.; Bohnert, E.; Rossberg, A.; Göttlicher, J.; Dardenne, K.; Rothe, J.; Schäfer, T.; Geckeis, H.; Vitova, T. Uranium Redox Transformations after U(VI) Coprecipitation with Magnetite Nanoparticles. *Environ. Sci. Technol.* **2017**, *51*, 2217–2225.

(32) Roberts, H. E.; Morris, K.; Law, G. T. W.; Mosselmans, J. F. W.; Bots, P.; Kvashnina, K.; Shaw, S. Uranium(V) Incorporation Mechanisms and Stability in Fe(II)/Fe(III) (Oxyhydr)Oxides. *Environ. Sci. Technol. Lett.* **2017**, *4*, 421–426.

(33) Partin, C. A.; Lalonde, S. V.; Planavsky, N. J.; Bekker, A.; Rouxel, O. J.; Lyons, T. W.; Konhauser, K. O. Uranium in Iron Formations and the Rise of Atmospheric Oxygen. *Chem. Geol.* **2013**, *362*, 82–90.

(34) Brennecka, G. A.; Wasylenko, L. E.; Bargar, J. R.; Weyer, S.; Anbar, A. D. Uranium Isotope Fractionation during Adsorption to Mn-Oxyhydroxides. *Environ. Sci. Technol.* **2011**, *45*, 1370–1375.

(35) Dang, D. H.; Novotnik, B.; Wang, W.; Georg, R. B.; Evans, R. D. Uranium Isotope Fractionation during Adsorption, (Co)-Precipitation, and Biotic Reduction. *Environ. Sci. Technol.* **2016**, *50*, 12695–12704.

(36) Ilton, E. S.; Boily, J.-F.; Buck, E. C.; Skomurski, F. N.; Rosso, K. M.; Cahill, C. L.; Bargar, J. R.; Felmy, A. R. Influence of Dynamical Conditions on the Reduction of UVI at the Magnetite-Solution Interface. *Environ. Sci. Technol.* **2010**, *44*, 170–176.

(37) Pan, Z.; Bártová, B.; LaGrange, T.; Butorin, S. M.; Hyatt, N. C.; Stennett, M. C.; Kvashnina, K. O.; Bernier-Latmani, R. Nanoscale Mechanism of UO₂ Formation through Uranium Reduction by Magnetite. *Nat. Commun.* **2020**, *11*, 1–12.

(38) Stagg, O.; Morris, K.; Lam, A.; Navrotsky, A.; Velazquez, J. M.; Schacherl, B.; Vitova, T.; Rothe, J.; Galanzew, J.; Neumann, A.; Lythgoe, P.; Abrahamsen-Mills, L.; Shaw, S. Fe (II) Induced Reduction of Incorporated U (VI) to U (V) in Goethite. *Environ. Sci. Technol.* **2021**, *55*, 16445–16454.

(39) Wan, J.; Tokunaga, T. K.; Brodie, E.; Wang, Z.; Zheng, Z.; Herman, D.; Hazen, T. C.; Firestone, M. K.; Sutton, S. R. Reoxidation of Bioreduced Uranium under Reducing Conditions. *Environ. Sci. Technol.* **2005**, *39*, 6162–6169.

(40) Richter, S.; Eykens, R.; Kühn, H.; Aregbe, Y.; Verbruggen, A.; Weyer, S. New Average Values for the n(238U)/n(235U) Isotope Ratios of Natural Uranium Standards. *Int. J. Mass Spectrom.* **2010**, *295*, 94–97.

(41) Senko, J. M.; Istok, J. D.; Sufliya, J. M.; Krumholz, L. R. In-Situ Evidence for Uranium Immobilization and Remobilization. *Environ. Sci. Technol.* **2002**, *36*, 1491–1496.

(42) Noordmann, J.; Weyer, S.; Montoya-Pino, C.; Dellwig, O.; Neubert, N.; Eckert, S.; Paetzel, M.; Böttcher, M. E. Uranium and Molybdenum Isotope Systematics in Modern Euxinic Basins: Case

Studies from the Central Baltic Sea and the Kyllaren Fjord (Norway). *Chem. Geol.* **2015**, *396*, 182–195.

(43) Roebbert, Y.; Rosendahl, C. D.; Brown, A.; Schippers, A.; Bernier-Latmani, R.; Weyer, S. Uranium Isotope Fractionation during the Anoxic Mobilization of Noncrystalline U(IV) by Ligand Complexation. *Environ. Sci. Technol.* **2021**, *55*, 7959–7969.

(44) Kleyenov, E.; Van Bokhoven, J. A.; David, C.; Glatzel, P.; Janousch, M.; Alonso-Mori, R.; Studer, M.; Willmann, M.; Bergamaschi, A.; Henrich, B.; Nachtegaal, M. Five-Element Johann-Type x-Ray Emission Spectrometer with a Single-Photon-Counting Pixel Detector. *Rev. Sci. Instrum.* **2011**, *82*, 06S107.

(45) Walshe, A.; Prüßmann, T.; Vitova, T.; Baker, R. J. An EXAFS and HR-XANES Study of the Uranyl Peroxides [UO₂(H₂O)₂·nH₂O (n = 0, 2) and Uranyl (Oxy)Hydroxide [(UO₂)₄O(OH)₆]·6H₂O. *Dalton Trans.* **2014**, *43*, 4400–4407.

(46) Glatzel, P.; Bergmann, U. High Resolution 1s Core Hole X-Ray Spectroscopy in 3d Transition Metal Complexes - Electronic and Structural Information. *Coord. Chem. Rev.* **2005**, *249*, 65–95.

(47) Zimina, A.; Dardenne, K.; Denecke, M. A.; Doronkin, D. E.; Huttel, E.; Lichtenberg, H.; Mangold, S.; Pruessmann, T.; Rothe, J.; Spangenberg, T.; Steininger, R.; Vitova, T.; Geckeis, H.; Grunwaldt, J.-D. CAT-ACT—A New Highly Versatile x-Ray Spectroscopy Beamline for Catalysis and Radionuclide Science at the KIT Synchrotron Light Facility ANKA. *Rev. Sci. Instrum.* **2017**, *88*, 113113.

(48) Huber, F.; Schild, D.; Vitova, T.; Rothe, J.; Kirsch, R.; Schäfer, T. U(VI) Removal Kinetics in Presence of Synthetic Magnetite Nanoparticles. *Geochim. Cosmochim. Acta* **2012**, *96*, 154–173.

(49) Soldatov, A. V.; Lamoen, D.; Konstantinović, M. J.; Van den Berghe, S.; Scheinost, A. C.; Verwerft, M. Local Structure and Oxidation State of Uranium in Some Ternary Oxides: X-Ray Absorption Analysis. *J. Solid State Chem.* **2007**, *180*, 54–61.

(50) Roßberg, A.; Reich, T.; Bernhard, G. Complexation of Uranium(VI) with Protocatechuic Acid—Application of Iterative Transformation Factor Analysis to EXAFS Spectroscopy. *Anal. Bioanal. Chem.* **2003**, *376*, 631–638.

(51) Popa, K.; Prieur, D.; Manara, D.; Naji, M.; Vigier, J.-F.; Martin, P. M.; Dieste Blanco, O.; Scheinost, A. C.; Prüßmann, T.; Vitova, T.; Raison, P. E.; Somers, J.; Konings, R. J. M. Further Insights into the Chemistry of the Bi–U–O System. *Dalton Trans.* **2016**, *45*, 7847–7855.

(52) Gorski, C. A.; Handler, R. M.; Beard, B. L.; Pasakarnis, T.; Johnson, C. M.; Scherer, M. M. Fe Atom Exchange between Aqueous Fe²⁺ and Magnetite. *Environ. Sci. Technol.* **2012**, *46*, 12399–12407.

(53) Handler, R. M.; Beard, B. L.; Johnson, C. M.; Scherer, M. M. Atom Exchange between Aqueous Fe(II) and Goethite: An Fe Isotope Tracer Study. *Environ. Sci. Technol.* **2009**, *43*, 1102–1107.

(54) Friedrich, A. J.; Helgeson, M.; Liu, C.; Wang, C.; Rosso, K. M.; Scherer, M. M. Iron Atom Exchange between Hematite and Aqueous Fe(II). *Environ. Sci. Technol.* **2015**, *49*, 8479–8486.

(55) Marshall, T. A.; Morris, K.; Law, G. T. W.; Livens, F. R.; Mosselmann, J. F. W.; Bots, P.; Shaw, S. Incorporation of Uranium into Hematite during Crystallization from Ferrihydrite. *Environ. Sci. Technol.* **2014**, *48*, 3724–3731.

(56) Wang, X.; Johnson, T. M.; Lundstrom, C. C. Isotope Fractionation during Oxidation of Tetravalent Uranium by Dissolved Oxygen. *Geochim. Cosmochim. Acta* **2015**, *150*, 160–170.

(57) Stadelmann, P. A. EMS - a Software Package for Electron Diffraction Analysis and HREM Image Simulation in Materials Science. *Ultramicroscopy* **1987**, *21*, 131–145.

(58) Planavsky, N. J.; Asael, D.; Hofmann, A.; Reinhard, C. T.; Lalonde, S. V.; Knudsen, A.; Wang, X.; Ossa Ossa, F.; Pecoits, E.; Smith, A. J. B.; Beukes, N. J.; Bekker, A.; Johnson, T. M.; Konhauser, K. O.; Lyons, T. W.; Rouxel, O. J. Evidence for Oxygenic Photosynthesis Half a Billion Years before the Great Oxidation Event. *Nat. Geosci.* **2014**, *7*, 283–286.



ACS IN FOCUS

Cellular Agriculture
Lab-Grown
Dilek Erilliç
Dorothee E.

Machine Learning in Chemistry
Jon Paul Janet & Heather J. Kulik

bacterials
Lidia Cheng Jaramillo
William M. Wuest

ACS Publications

ACS In Focus ebooks are digital publications that help readers of all levels accelerate their fundamental understanding of emerging topics and techniques from across the sciences.

pubs.acs.org/series/infocus

ACS Publications
Most Trusted. Most Cited. Most Read.

<https://doi.org/10.1021/acs.est.1c06865>
Environ. Sci. Technol. XXXX, XXX, XXX–XXX